Photon Reabsorption in Mixed CsPbCl₃:CsPbI₃ Perovskite Nanocrystal Films for Light-Emitting Diodes

Nathaniel J. L. K. Davis,[†] Francisco J. de la Peña,[‡] Maxim Tabachnyk,[†] Johannes M. Richter,[†] Robin D. Lamboll,[†] Edward P. Booker,[†] Florencia Wisnivesky Rocca Rivarola,[‡] James T. Griffiths,[‡] Caterina Ducati,[‡] S. Matthew Menke,[†] Felix Deschler,[†] and Neil C. Greenham*,[†]

[†]Cavendish Laboratory, University of Cambridge, J.J. Thomson Avenue, Cambridge, CB3 0HE, U.K.

[‡]Department of Materials Science and Metallurgy, University of Cambridge, 27 Charles Babbage Road, Cambridge, CB3 0FS, U.K.

Ⓢ *Supporting Information*

ABSTRACT: Cesium lead halide nanocrystals, CsPbX₃ (X = Cl, Br, I), exhibit photoluminescence quantum efficiencies approaching 100% without the core−shell structures usually used in conventional semiconductor nanocrystals. These high photoluminescence efficiencies make these crystals ideal candidates for light-emitting diodes (LEDs). However, because of the large surface area to volume ratio, halogen exchange between perovskite nanocrystals of different compositions occurs rapidly, which is one of the limiting factors for white-light applications requiring a mixture of different crystal compositions to achieve a broad emission spectrum. Here, we use mixtures of chloride and iodide CsPbX₃ (X = Cl, I) perovskite nanocrystals where anion exchange is significantly reduced. We investigate samples containing mixtures of perovskite nanocrystals with different compositions and study the resulting optical and electrical interactions. We report excitation transfer from CsPbCl₃ to CsPbI₃ in solution and within a poly(methyl methacrylate) matrix via photon reabsorption, which also occurs in electrically excited crystals in bulk heterojunction LEDs.
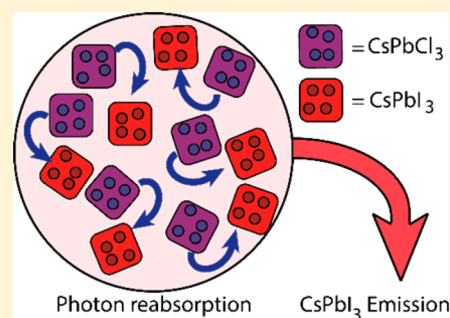
INTRODUCTION

Low-cost solution-processable metal halide perovskite semiconductors[1−4] have seen encouraging development as inexpensive absorber layers in solar cells, and show high mobility,[5−7] bright emission,[8] tunable band gap,[9−11] and photon recycling.[12] Power conversion efficiencies for perovskite solar cells have exceeded 20%.[13−16] While the majority of research has focused on thin-film and bulk materials,[4,15,17] perovskite nanocrystals have recently been synthesized. These include hybrid organic−inorganic MAPbX₃ (MA = methylammonium, X = Cl, Br, I) nanocrystals and nanostructures as well as all-inorganic cesium lead halide CsPbX₃ (X = Cl, Br, I) and cesium tin halide CsSnX₃ (X = Cl, Br, I) nanocrystals and nanostructures.[18−20] The move to colloidal semiconductor quantum dots not only improves solution processability of these materials but also allows band gap tunabilty due to three-dimensional (3D) confinement effects,[19,21] and creates a material that is readily miscible with other optoelectronic materials, for example, polymers, fullerenes, and other nanomaterials. Hybrid organic−inorganic lead halide perovskite nanostructures have been used in detectors for the visible, ultraviolet, and X-ray regions of the electromagnetic spectrum,[22,23] as gain media for optically pumped lasers,[10,24−28] and as emission layers for light-emitting diodes (LEDs).[8,29]

It has been reported that in perovskites ABX₃ (A = MA, Cs; B = Pb, Sn; X = Cl, Br, I) the ratios of the different halide components have a strong influence on the electronic properties of the material.[30] The ability of the halide ions to migrate within bulk perovskite has been reported both for MAPbX₃[31,32] and for CsPbX₃,[33,34] which has specifically been identified as a halide-ion conductor.[35] The high ion mobility within perovskite crystals has been recognized as a possible source for the hysteresis in the current−voltage curves seen in photovoltaic devices.[36] In CsPbX₃ nanocrystals, which have a high surface area to volume ratio, halide exchange quickly incorporates new sources of excess halides, resulting in a shift of the optical band gap. This is also the case when crystals with different halide compositions are mixed, resulting in the formation of crystals with an averaged total halide composition.[33,34] Halide exchange has been shown to be possible in both MAPbX₃ and CsPbX₃ when moving between periodically adjacent halides, for example, from CsPbCl₃ to CsPbBr₃ and CsPbBr₃ to CsPbI₃ and vice versa.[33,34]

Although recently there has been an increase in the application of CsPbX₃ nanocrystals,[24,37−40] the inability of CsPbX₃ nanocrystals with different compositions to coexist as discrete semiconductors in one sample without rapid halide exchange significantly limits their use in applications where multiple band gaps are required, such as white-light LEDs and

exciton concentration systems. Recently, Palazon et al.[41] showed that cross-linking the surface ligands in neat nanocrystal films improves stability, prevents film liftoff, and limits halogen exchange. It has also been shown that wrapping clusters of CsPbX$_3$ nanocrystals in polyhedral oligomeric silsesquioxane cages can prevent halogen exchange.[42] However, neither of these methods allows the formation of films where the nanocrystals are mixed on the submicrometer scale.

Energy transfer from high band gap to low band gap nanocrystals has been demonstrated between CsPbBr$_3$ particles of different sizes.[43] Interactions between CsPbCl$_3$ and CsPbI$_3$ nanocrystals have previously been reported to lead to dissolution of the nanocrystals.[33] We find that when the crystals are synthesized and kept in an oxygen- and water-free environment, this is not the case, consistent with a recent report by Dastidar et al.[44] We report significantly reduced halide exchange between chloride and iodide in CsPbX$_3$ (X = Cl, I) perovskite nanocrystals because of the unfavorable crystal lattice tolerance factor for iodide–chloride exchange in this system. This allows us to investigate films and solutions containing nanocrystals of differing compositions, and to study the resulting optical and electronic interactions. Efficient excitation transfer from CsPbCl$_3$ to CsPbI$_3$ is found to proceed by a radiative process. Excitation transfer also occurs in electrically pumped crystals forming the active layer of a bulk heterojunction LED. CsPbCl$_3$ emission can efficiently be reabsorbed by the CsPbI$_3$ nanocrystals and re-emitted in the red region.

■ METHODS

All chemicals were purchased from Sigma-Aldrich (St. Louis) and were used as-received.

Synthesis of CsPbX$_3$ (X = Cl, I) Nanocrystals. Perovskite nanocrystals were synthesized using previously reported procedures.[19] Cs$_2$CO$_3$ (0.814g, 99.9%) was loaded into 100 mL three-neck flask along with octadecene (ODE, 30 mL, 90%) and oleic acid (2.5 mL, OA, 90%), and the mixture was dried for 2 h at 120 °C under N$_2$. The solution temperature was then lowered to 100 °C. ODE (75 mL), oleylamine (7.5 mL, OLA, 90%), and dried OA (7.5 mL) and PbX$_2$ (2.82 mmol) such as PbI$_2$ (1.26 g, 99.99%) and PbCl$_2$ (0.675g, 99.99%), were loaded into a 250 mL three-neck flask and dried under vacuum for 2 h at 120 °C. After complete solubilization of the PbX$_2$ salt, the temperature was raised to 170 °C and the Cs–oleate solution (6.0 mL, 0.125 M in ODE, prepared as-described above) was quickly injected. After 10 s, the reaction mixture was cooled in an ice–water bath. For CsPbCl$_3$ synthesis, 5 mL of trioctylphosphine (TOP, 97%) was added to solubilize PbCl$_2$. The nanocrystals were transferred to an argon-gloved box (H$_2$O and O$_2$ < 1 ppm) and precipitated from solution by the addition of equal volume anhydrous butanol (BuOH, 99%) (ODE:BuOH = 1:1 by volume). After centrifugation, the supernatant was discarded and the nanocrystals were redispersed in anhydrous hexane (99%) and precipitated again with the addition of BuOH (hexane:BuOH = 1:1 by volume). These were redispersed in hexane. The nanocrystal dispersion was filtered through a 0.2 μm polytetrafluoroethylene filter and diluted to 10 mg mL^{-1} in hexane before use. Subsequent mixing was carried out in a nitrogen-filled glove box, and under these conditions the mixed solutions were stable for at least 2 months at −19 °C. Exposure of mixed solutions to ambient conditions led to rapid dissolution of the CsPbI$_3$ particles.

Continuous Wave Measurements. Absorption spectra of solutions were measured on nanocrystals samples dispersed in hexane at a concentration of ca. 1 mg mL^{-1} in a 1 cm × 1 cm cuvette using a HP 8453 spectrometer. Film absorption spectra were measured on a HP 8453 spectrometer. The samples were prepared on quartz glass by spin-coating from 10 mg mL^{-1} solutions at 2000 rpm for 15 s, or for polymer samples a 10 mg mL^{-1} perovskite nanocrystal dispersion in 10 mg mL^{-1} poly(9-vinylcarbazole) (PVK) in toluene was spin-coated at 2000 rpm for 60 s. Photoluminescence was measured on an Edinburgh Instruments FLS980 fluorimeter. Solution samples were measured in a 1 cm × 0.3 cm cuvette excited in the 1 cm direction and imaged in the 0.3 cm direction. Film samples were excited by front face illumination at 45° to the surface; detection was at 90° to excitation and also at 45° to the surface.

Monte Carlo Simulations. A Monte Carlo simulation of the expected photoluminescence (PL) was constructed, using only the measured emission and absorption spectra of the constituent species. Photons are generated, traveling in random directions from the middle axis. The model is two-dimensional, allowing light to leave the system in either the small or large axis, with dimensions of 0.3 or 3 cm. Photon travel lengths are randomly generated, consistent with the concentration- and wavelength-dependent absorption lengths arising from the two species in the mix. The travel distance is then the shorter of these two distances. If this length takes the photon outside the container, it is counted toward the final spectrum if it leaves via the small axis and ignored if it leaves via the large axis. Otherwise, it has a chance equal to the pure substance photoluminescence quantum efficiency (PLQE) of being re-emitted by the species that absorbed it, in a new random direction and according to that species' emission spectrum. All values required can be measured from the single-species solutions, and so the model contains no fitted parameters.

Time-Correlated Single-Photon Counting (TCSPC) Measurements. The samples were prepared on quartz glass by spin coating from a 10 mg mL^{-1} perovskite nanocrystal dispersion in 10 mg mL^{-1} PVK in toluene at 2000 rpm for 60 s. The nanocrystal films were encapsulated by affixing a glass coverslip on the nanocrystal layer using carbon tape as a spacer unit and epoxy glue as a sealant. The samples were excited by front face illumination at 45° to the surface; detection was at 90° to excitation and also at 45° to the surface.

Transmission Electron Microscopy (TEM). TEM samples were prepared by drop-casting an ca. 40 mg mL^{-1} perovskite crystals solution in octane on a TEM Grid (200 mesh Cu, Agar Scientific) in a argon-filled glove box. High-angle annular dark field scanning transmission electron microscopy (HAADF-STEM) and electron energy loss spectroscopy (EELS) analysis were also conducted on a FEI Tecnai Osiris TEM/STEM 80-200 microscope, operating at 80 kV, using a liquid nitrogen holder, and equipped with a Gatan Enfinium ER 977 spectrometer with dual EELS. The convergence and collection angles used were 8.5 and 34 mrad, respectively. The EELS spectral images were analyzed using principal component analysis and the elemental maps with the absolute quantification were obtained through the use of the integration method proposed by Egerton.[45] The EELS data analysis and elemental quantification were performed using the open source software package HyperSpy toolbox.

X-ray Diffraction (XRD). Perovskite nanocrystal films were prepared by drop-casting a 10 mg mL^{-1} nanocrystals solution in hexane on silicon wafers. XRD experiments were carried out on a Bruker X-ray diffractometer using a Cu Kα radiation source (λ = 1.5418 Å). The measurements were taken from 2θ of 10°−70° with a step size of 0.0102° in 2θ.

Film Thickness. Film thicknesses were measured using a DEKTAK profilometer and a Digital Instruments/Veeco Dimension 3100 atomic force microscope.

PLQE Measurements. Nanocrystal films were placed in an integrating sphere and were photoexcited using a 405 nm continuous-wave laser. The laser and the emission signals were measured and quantified using a calibrated Andor iDus DU490A InGaAs detector for the determination of PL quantum efficiency. PLQE was calculated as per de Mello et al.[46]

LED Device Fabrication. Poly(3,4-ethylenedioxythiophene):polystyrenesulfonate (PEDOT:PSS) was spin-coated onto an indium−tin oxide (ITO)-coated glass substrate at 6000 rpm for 45 s, followed by annealing at 140 °C for 30 min in a nitrogen-filled glove box. A 10 mg mL^{-1} perovskite nanocrystal dispersion in 10 mg mL^{-1} PVK in toluene was spin-coated at 2000 rpm for 60 s in an argon-filled glove box to give a 50−60 nm film. The samples were then transferred into a thermal evaporator, and calcium (Ca; 20 nm) and silver (Ag; 80 nm)
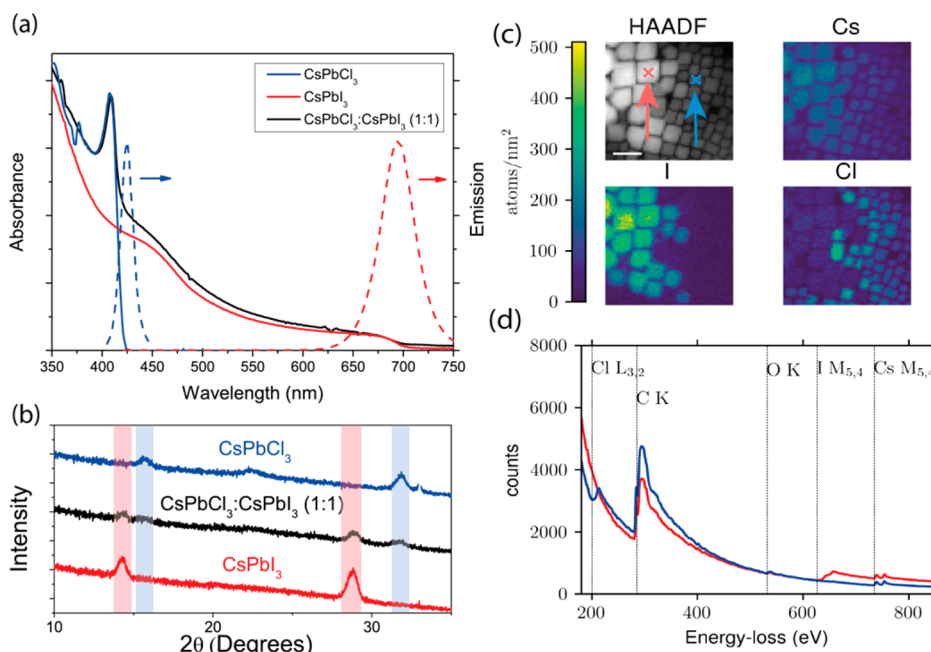
Figure 1. (a) Absorption spectra (left) of pure $CsPbCl_3$, $CsPbI_3$, and a 1:1 nanocrystal blend and emission spectra (right) of pure $CsPbCl_3$ and $CsPbI_3$ in hexane (concentration $\approx$1 mg mL^{-1}). (b) Powder XRD patterns of $CsPbCl_3$, $CsPbI_3$, and 1:1 nanocrystal blend solid films with distinctive peak highlighted. (c) HAADF TEM images and EELS TEM maps for Cs, I, and Cl. Scale bar = 20 nm. (d) EELS TEM spectrum for $CsPbCl_3$:$CsPbI_3$ (1:1) samples taken at the positions of the red and blue crosses in (c). Lines indicate atomic absorption edges.

were deposited through a shadow mask at 3×10^{-6} mbar or better. The LEDs were encapsulated by affixing a glass slide on top of the contacts using transparent ultraviolet (UV) epoxy glue.

LED Characterization. Current versus voltage characteristics were measured using a Keithley 2400 source measure unit. Photon flux was measured simultaneously using a calibrated silicon photodiode centered over the light-emitting pixel. Luminance in cd m^{-2} was calculated based on the emission spectrum of the LED, weighted against the standard luminosity function and on the known spectral response of the silicon photodiode. External quantum efficiency was calculated assuming a Lambertian emission profile. Electroluminescence spectra were measured using a Labsphere CDS-610 spectrometer.

⬛ RESULTS AND DISCUSSION

$CsPbX_3$ (X = Cl, I) nanocrystals were prepared as previously reported by Protesescu et al.[19] (details in the Methods section). All processing and characterization were performed in an inert atmosphere (oxygen and water <5 ppm). Under these conditions we find that $CsPbCl_3$ and $CsPbI_3$ nanocrystals coexist in solution without undergoing dissolution or significant halogen exchange. To investigate the optical properties of this system, we prepared solutions of $CsPbCl_3$ and $CsPbI_3$ at an overall crystal concentration of $\approx$1 mg mL^{-1} (Figure 1a). The respective absorbance spectra are shown in Figure 1a. We find absorbance onsets of 425 and 690 nm for the $CsPbCl_3$ and $CsPbI_3$ samples, respectively. The $CsPbCl_3$ nanocrystals show a sharp peak close to the absorption onset, which likely arises from excitonic effects. Mixed solutions show a combination of the characteristic features of the pure nanocrystal solutions without any spectral shifting. By fitting the absorbance spectrum of the mixed solution with a sum of the pure sample spectra, we calculate the ratio of the different crystals in a nominally 1:1 mixed solution sample to be 1:0.957 ($CsPbCl_3$:$CsPbI_3$) (Figure 1 of the Supporting Information). To investigate the structural and physical properties of the

mixed system by powder XRD and TEM, neat films of the crystals were drop-cast from a 10 mg mL^{-1} solution respectively onto silicon and onto carbon-coated copper substrates. The XRD pattern (Figure 1b) shows peaks at 16° and 32.5° corresponding to those found in pure $CsPbCl_3$ crystals reported by Protesescu et al.[19] and similarly at 14° and 28° in the pure $CsPbI_3$ crystals. The XRD pattern of the $CsPbCl_3$:$CsPbI_3$ (1:1) sample is a superposition of the $CsPbCl_3$ and $CsPbI_3$ nanocrystal XRD patterns. The presence of both $CsPbCl_3$ and $CsPbI_3$ peaks in the blends, without any shifts or additional peaks, indicates that these crystal structures exist in parallel in our nanocrystal blend films. HAADF TEM imaging (Figure 1c) shows two distinct types of nanocrystals with slightly different contrasts and sizes, suggesting two different nanocrystal populations. EELS and scanning transmission electron microscopy (STEM) was then used to further assign these crystal populations and obtain an absolute quantification of each element. The individual elemental maps with number of atoms per nm^2, shown in Figure 1c, indicate that the iodide is localized on the larger crystals while the chloride is localized on the smaller crystals. The amount of I and Cl in the nanocrystals maintains a 3:1 stoichiometric ratio with Cs. The EELS spectra measured at the two locations in Figure 1c show two distinct traces for different nanocrystal populations and are shown in Figure 1d. The blue trace, corresponding to EELS measurements at the blue cross, is assigned to a $CsPbCl_3$ nanocrystal with edges seen for Cs, C, Cl, and O, and the red trace, corresponding to EELS measurements at the red cross, is assigned to a $CsPbI_3$ nanocrystal with edges seen for Cs, C, I, and O. The sizes of the $CsPbCl_3$ and $CsPbI_3$ nanocrystals were measured at 7.0 ± 2.8 and 12.0 ± 3.9 nm, respectively. These data confirm that the $CsPbCl_3$ and $CsPbI_3$ nanocrystals are intimately mixed but remain discrete entities with insignificant halide mixing between them. The data in Figure 1 support our conclusion that $CsPbCl_3$ and $CsPbI_3$ do not undergo significant
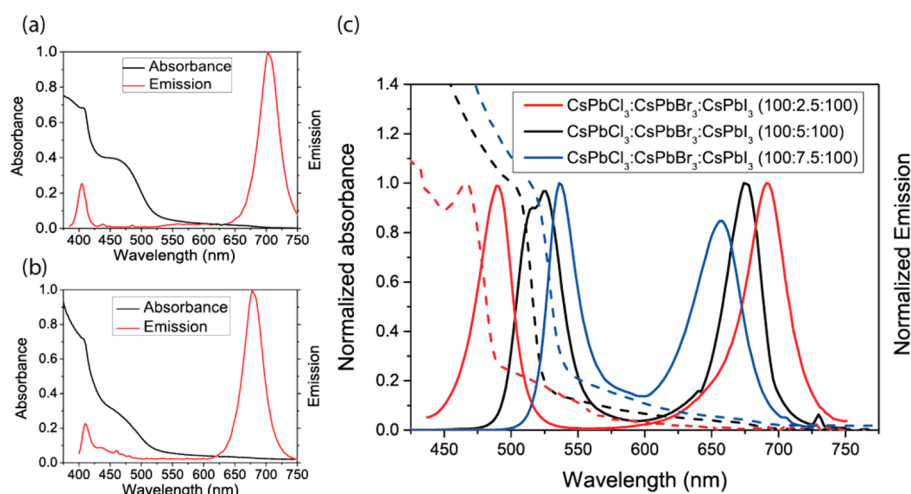
Figure 2. (a) Solid-state absorbance and emission spectra of $CsPbCl_3$:$CsPbI_3$ (1:1) in PMMA, film thickness $\approx$20 nm (10 mg mL^{-1} nanocrystals and 10 mg mL^{-1} PMMA in toluene, spun at 6000 rpm). (b) Solid state absorbance and emission in neat mixed crystal films (10 mg mL^{-1} in toluene, spun at 2000 rpm). (c) Absorbance and emission of $\approx$0.1 mg mL^{-1} nanocrystals in toluene) with different $CsPbCl_3$:$CsPbBr_3$:$CsPbI_3$ ratios.
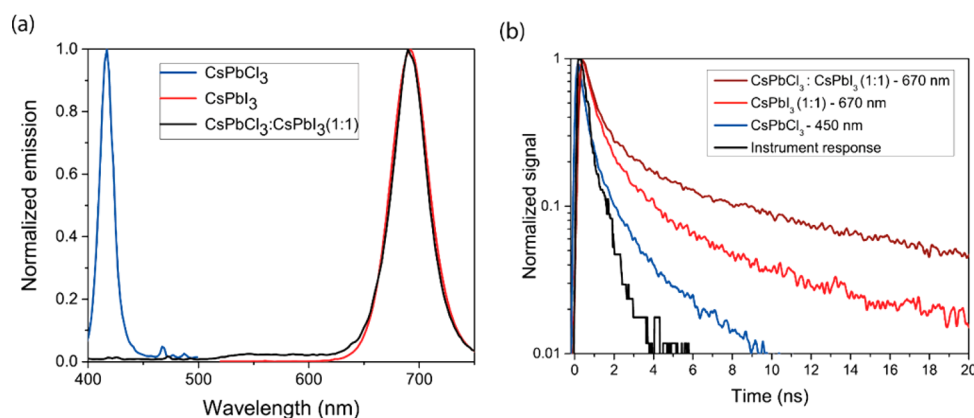

Figure 3. (a) Luminescence of $CsPbCl_3$, $CsPbI_3$, and $CsPbCl_3$:$ClPbI_3$ blends in PMMA matrix at a total nanocrystal:polymer ratio of 1:1 by weight and film thickness $\approx$75 nm. (b) Transient luminescence decays excited at 405 nm with measurements at 450 or 670 nm.

halogen exchange with each other. The lack of halogen exchange in these systems is assigned to the different tolerance factors of the different crystal lattices acting to inhibit halogen exchange.[47]

The ability of these crystals to exist as discrete entities gives us the unique opportunity to study these crystals and their photophysical interactions with each other. $CsPbCl_3$ nanocrystals emit in the near UV at 425 nm, whereas $CsPbI_3$ nanocrystals emit in the red at 695 nm (Figure 1a). When excited at 365 nm, nanocrystals dispersed in a poly(methyl methacrylate) (PMMA) matrix at a total nanocrystal:polymer ratio of 1:1 by weight (film thickness $\approx$20 nm) (Figure 2a) and neat mixed nanocrystal films spun from toluene (Figure 2b) clearly show emission from both types of nanocrystals. Spectral tuning of the separate crystals was also achievable by incorporating a small (weight fraction $\leq$10%) amount of $CsPbBr_3$ nanocrystals in a solution of $CsPbCl_3$ and $CsPbI_3$ nanocrystals. As there is not enough $CsPbBr_3$ to represent a majority, the $CsPbBr_3$ is incorporated into the $CsPbCl_3$ and $CsPbI_3$ crystals, resulting in a $CsPbCl_{(3-x)}Br_x$ and $CsPbI_{(3-x)}Br_x$ blend (Figure 2c).

When the crystals were excited directly at 550 nm, the overall PLQE yield of the $CsPbI_3$ crystals decreased with increasing $CsPbCl_3$ ratios (Figure 2 of the Supporting Information).

Despite there being no change in XRD (Figure 3 of the Supporting Information) or the emission spectrum, TEM images show a small amount of migration of chloride ions into the $CsPbI_3$ crystals (Figure 1c; Figure 4 of the Supporting Information). We attribute the decrease in PLQE to small amounts of chloride migration which increases the amount of nonradiative decay within the crystals. This is consistent with TCSPC measurements (Figure 5 of the Supporting Information), which show the $CsPbI_3$ fluorescence decay lifetimes are shortened for ratios greater that 1:1. We are still able to achieve high PLQEs in the $CsPbI_3$ nanocrystals at a 1:1 ratio.

The above spectra (Figure 2a,b) showed emission from both $CsPbCl_3$ and $CsPbI_3$ nanocrystals; however, when $CsPbCl_3$ and $CsPbI_3$ nanocrystals are mixed in a 1:1 ratio at higher solution concentrations and in thicker polymer matrixes, the emission was found to be predominantly at 695 nm under 405 nm excitation. Solutions of $CsPbCl_3$ and $CsPbCI_3$ nanocrystals showed emission solely from the $CsPbI_3$ crystals up until a 20-fold excess of $CsPbCl_3$ (Figure 6 of the Supporting Information). Emission solely from the low-energy particles was also seen for nanocrystals dispersed in a PMMA matrix at a total nanocrystal:polymer ratio of 1:1 by weight and film thickness $\approx$75 nm (Figure 3a). These results indicate that there is efficient energy transfer to the low-energy nanocrystals.
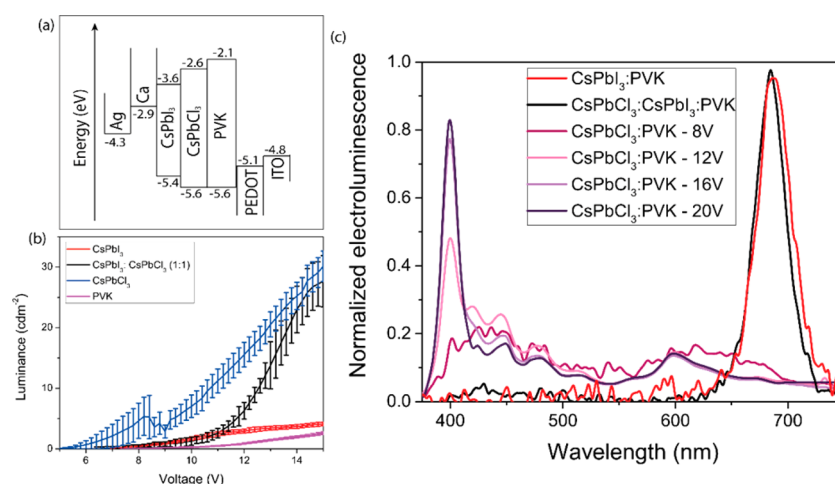
Figure 4. (a) Band diagram and structure of the bulk heterojunction LEDs. (b) Change in luminance with voltage in the bulk heterojunction LEDs. (c) Electroluminescence spectra of $CsPbI_3$:PVK, $CsPbCl_3$:$CsPbI_3$:PVK, and $CsPbCl_3$:PVK at different voltages. The electroluminescence spectra of the $CsPbI_3$:PVK and $CsPbCl_3$:$CsPbI_3$:PVK remain constant with voltage (not shown).

The interaction responsible for this energy transfer in solid films was investigated through transient spectroscopy techniques. For mixed samples with a 1:1 ratio of $CsPbCl_3$:$CsPbI_3$ by weight, the $CsPbI_3$ nanocrystals show an increased lifetime when excited at 405 nm compared to pure $CsPbI_3$ samples (Figure 3b). Consistent with steady state measurements, there was no emission from the $CsPbCl_3$ nanocrystals in the mixed samples. An extended luminescence lifetime in the lower-energy particle is consistent with excitation transfer. One possible mechanism for this energy transfer is Förster resonance energy transfer (FRET). We calculate the Förster radius R_0, the distance at which 50% of all excitations lead to energy transfer from the donor to the acceptor,[48] using measured absorption, emission, and PLQE data to be 6.8 ± 0.3 nm. This value is comparable to the size of the nanocrystals so the point dipole approximation stipulated in FRET calculations is not entirely appropriate. It is also worth noting that the large aliphatic ligands that offer colloidal stability are still attached to these crystals. This combined with the apparent slight phase separation of the two crystals in neat films (Figure 1c; Figure 4 of the Supporting Information) and the fact that the crystals are supported in a polymer matrix means that the distance between a $CsPbCl_3$ and $CsPbI_3$ particle is generally greater than 6.8 nm. We cannot completely rule out FRET playing a role in energy transfer, but crucially the fact that energy transfer is more complete in thick films, with the same interparticle spacing, suggests that another mechanism is dominating. We therefore ascribe the dominant emission from $CsPbI_3$ nanocrystals in $CsPbCl_3$:$CsPbI_3$ blends to efficient reabsorption of photons emitted from $CsPbCl_3$ nanocrystals. A Monte Carlo algorithm allowing for multiple absorption and re-emission events gives an accurate replication of the measured emission in concentrated solutions and shows the measured down conversion of the blue emission to red (Figure 7 of the Supporting Information).

To use the potential of this efficient photon reabsorption between different $CsPbX_3$ (X = Cl, I) nanocrystals, we incorporated them into bulk heterojunction polymer/$CsPbX_3$ nanocrystal LEDs. The LEDs were made by spin-coating PEDOT:PSS on an ITO glass substrate. A toluene solution containing 10 mg mL^{-1} nanocrystal and 10 mg mL^{-1} PVK was further spun on top, giving a 50−60 nm film, and a calcium and silver electrode was deposited by thermal evaporation (Figure 4a). Devices of $CsPbCl_3$, $CsPbI_3$, $CsPbCl_3$:$CsPbI_3$ (1:1) (all in PVK matrixes), and pure PVK were produced.

All devices were inefficient, with quantum efficiencies less than 0.04% (Figure 8a of the Supporting Information), and relatively high voltages were required to achieve significant luminances (Figure 4b). Devices containing PVK showed broad emission, consistent with previous reports,[49,50] and had the highest current densities (Figure 8b). Adding $CsPbCl_3$ particles had only a minor effect on the current density (Figure 8b), but at high voltages led to a clear emission peak around 400 nm (Figure 4c), consistent with charge capture and recombination occurring on the particles. With $CsPbI_3$ particles, the emission was solely from the particles, centered around 695 nm (Figure 4c), but the current density was reduced by an order of magnitude (Figure 8b), consistent with trapping of one or both carriers on the particles. Mixed $CsPbCl_3$:$CsPbI_3$/PVK devices maintain the high current densities comparable to those of the PVK and $CsPbCl_3$/PVK devices but show emission solely from the $CsPbI_3$ nanocrystals (Figure 4c; Figure 8b of the Supporting Information). This suggests that transport is dominated by the $CsPbCl_3$ particles but that any emission occurring from the $CsPbCl_3$ particles is converted to $CsPbI_3$ emission through photon reabsorption as demonstrated in the optical measurements described above. Devices containing mixed nanoparticles therefore show the best device performance. It would be attractive to obtain a mixture of blue and red emission in LEDs, which would require thinner films of mixed nanoparticles to avoid complete reabsorption of the blue emission as demonstrated optically in Figure 2. Unfortunately, though, we have not yet been able to fabricate working LEDs with active layer thicknesses below 40 nm.

■ CONCLUSION

In conclusion, we present the study of interactions in blends films with mixtures of different $CsPbX_3$ (X = Cl, I) perovskite nanocrystals. We find that $CsPbCl_3$ and $CsPbI_3$ nanocrystals can exist as discrete entities in solution, embedded in a polymer matrix and as neat films. The $CsPbCl_3$ emission can be reabsorbed by the $CsPbI_3$ nanocrystals due to the large absorption coefficient of the $CsPbI_3$ nanocrystals in the range of the $CsPbCl_3$ emission. This phenomenon can be utilized in

bulk heterojunction LEDs where the luminance of devices emitting in the 695 nm region can be improved by the incorporation of $CsPbCl_3$ nanocrystals. This causes the devices to operate at a higher current density with photon reabsorption transfer occurring from the $CsPbCl_3$ nanocrystals to the $CsPbI_3$ crystal for efficient re-emission.

■ ASSOCIATED CONTENT

Ⓢ Supporting Information

The data underlying this publication are available at https://doi.org/10.17863/CAM.7087. The Supporting Information is available free of charge on the ACS Publications website at DOI: 10.1021/acs.jpcc.6b12828.

Figure S1: Measured absorbance and modeled absorbance spectrum of the mixed 1:1 solutions. Figure S2: Photoluminescence quantum efficiency of different $CsPbCl_3$:$CsPbI_3$ blend ratios in PMMA. Figure S3: Powder X-ray diffraction pattern of different $CsPbCl_3$:$CsPbI_3$ blend ratios in PMMA. Figure S4: Two different HAADF and EELS TEM scans of different regions. Figure S5: Transient decays for different nanocrystal polymer films excited at 405 nm and measured at 450 and 670 nm. Figure S6: Solution absorbance and emission of $CsPbCl_3$:$ClPbI_3$ blends in hexane. Figure S7: Monte Carlo simulations of emission spectra from different nanocrystal solutions with different $CsPbCl_3$:$CsPbI_3$ ratios. Figure S8: External quantum efficiencies of LED devices and current density/voltage characteristic of LED devices (PDF)

■ AUTHOR INFORMATION

Corresponding Author

*E-mail: ncg11@cam.ac.uk. Phone: +44 (0)1223 766301.

ORCID Ⓞ

James T. Griffiths: 0000-0002-1198-1372

S. Matthew Menke: 0000-0003-4468-0223

Neil C. Greenham: 0000-0002-2155-2432

Author Contributions

N.J.L.K.D. synthesized and characterized the nanocrystals and carried out all experiments unless mentioned otherwise. M.T. and J.R. performed the transient photoluminescence measurements. E.B. performed the XRD measurements. S.M.M. performed the PLQE measurements. F.W.R.R., F.P.M, J.G., and C.D. performed the TEM measurements. R.D.L. carried out the Monte Carlo simulation. N.J.L.K.D., F.D., and N.C.G. contributed to writing the manuscript. All authors contributed to discussion and analysis of the results.

Notes

The authors declare no competing financial interest.

■ ACKNOWLEDGMENTS

■ REFERENCES

(1) Kojima, A.; Teshima, K.; Shirai, Y.; Miyasaka, T. Organometal Halide Perovskites as Visible-Light Sensitizers for Photovoltaic Cells. *J. Am. Chem. Soc.* **2009**, *131*, 6050−6051.

(2) Lee, M.; Teuscher, J.; Miyasaka, T.; Murakami, T. N.; Snaith, H. J. Efficient Hybrid Solar Cells Based on Meso-Superstructured Organometal Halide Perovskites. *Science* **2012**, *338*, 643−647.

(3) Burschka, J.; Pellet, N.; Moon, S.-J.; Humphry-Baker, R.; Gao, P.; Nazeeruddin, M. K.; Grätzel, M. Sequential Deposition as a Route to High-Performance Perovskite-Sensitized Solar Cells. *Nature* **2013**, *499*, 316−319.

(4) Nie, W.; Tsai, H.; Asadpour, R. High-Efficiency Solution-Processed Perovskite Solar Cells with Millimeter-Scale Grains. *Science* **2015**, *347*, 522−525.

(5) Stranks, S.; Eperon, G.; Grancini, G.; Menelaou, C.; Alcocer, M. J. P.; Leijtens, T.; Herz, L. M.; Petrozza, A.; Snaith, H. J. Electron-Hole Diffusion Lengths Exceeding 1 Micrometer in an Organometal Trihalide Perovskite Absorber. *Science* **2013**, *342*, 341−344.

(6) Xing, G.; Mathews, N.; Sun, S.; Lim, S.; Lam, Y. M.; Gratzel, M.; Mhaisalkar, S.; Sum, T. C. Long-Range Balanced Electron- and Hole-Transport Lengths in Organic-Inorganic $CH_3NH_3PbI_3$. *Science* **2013**, *342*, 344−347.

(7) Dong, Q.; Fang, Y.; Shao, Y.; Mulligan, P.; Qiu, J.; Cao, L.; Huang, J. Electron-Hole Diffusion Lengths > 175 um in Solution-Grown $CH_3NH_3PbI_3$ Single Crystals. *Science* **2015**, *347*, 967−970.

(8) Tan, Z.-K.; Moghaddam, R. S.; Lai, M. L.; Docampo, P.; Higler, R.; Deschler, F.; Price, M.; Sadhanala, A.; Pazos, L. M.; Credgington, D.; et al. Bright Light-Emitting Diodes Based on Organometal Halide Perovskite. *Nat. Nanotechnol.* **2014**, *9*, 687−692.

(9) Zhang, W.; Anaya, M.; Lozano, G.; Calvo, M. E.; Johnston, M. B.; Míguez, H.; Snaith, H. J. Highly Efficient Perovskite Solar Cells with Tunable Structural Color. *Nano Lett.* **2015**, *15*, 1698−1702.

(10) Xing, G.; Mathews, N.; Lim, S. S.; Yantara, N.; Liu, X.; Sabba, D.; Grätzel, M.; Mhaisalkar, S.; Sum, T. C. Low-Temperature Solution-Processed Wavelength-Tunable Perovskites for Lasing. *Nat. Mater.* **2014**, *13*, 476−480.

(11) Filip, M. R.; Eperon, G. E.; Snaith, H. J.; Giustino, F. Steric Engineering of Metal-Halide Perovskites with Tunable Optical Band Gaps. *Nat. Commun.* **2014**, *5*, 5757−5766.

(12) Pazos-Outón, L. M.; Szumilo, M.; Lamboll, R.; Richter, J. M.; Crespo-Quesada, M.; Abdi-Jalebi, M.; Beeson, H. J.; Vrucinic, M.; Alsari, M.; Snaith, H. J.; et al. Photon Recycling in Lead Iodide Perovskite Solar Cells. *Science* **2016**, *351*, 1430−1433.

(13) Green, M. A.; Ho-Baillie, A.; Snaith, H. J. The Emergence of Perovskite Solar Cells. *Nat. Photonics* **2014**, *8*, 506−514.

(14) Park, N.-G. Organometal Perovskite Light Absorbers toward a 20% Efficiency Low-Cost Solid-State Mesoscopic Solar Cell. *J. Phys. Chem. Lett.* **2013**, *4*, 2423−2429.

(15) Zhou, H.; Chen, Q.; Li, G.; Luo, S.; Song, T.-b.; Duan, H.-S.; Hong, Z.; You, J.; Liu, Y.; Yang, Y. Interface Engineering of Highly Efficient Perovskite Solar Cells. *Science* **2014**, *345* (6196), 542−546.

(16) Jeon, N. J.; Noh, J. H.; Yang, W. S.; Kim, Y. C.; Ryu, S.; Seo, J.; Seok, S. Il. Compositional Engineering of Perovskite Materials for High-Performance Solar Cells. *Nature* **2015**, *517*, 476−480.

(17) Shi, D.; Adinolfi, V.; Comin, R.; Yuan, M.; Alarousu, E.; Buin, A.; Chen, Y.; Hoogland, S.; Rothenberger, A.; Katsiev, K.; et al. Low Trap-State Density and Long Carrier Diffusion in Organolead

Trihalide Perovskite Single Crystals. *Science* **2015**, *347* (6221), 519−522.

(18) Zhang, D.; Eaton, S. W.; Yu, Y.; Dou, L.; Yang, P. Solution-Phase Synthesis of Cesium Lead Halide Perovskite Nanowires. *J. Am. Chem. Soc.* **2015**, *137*, 9230−9233.

(19) Protesescu, L.; Yakunin, S.; Bodnarchuk, M. I.; Krieg, F.; Caputo, R.; Hendon, C. H.; Yang, R. X.; Walsh, A.; Kovalenko, M. V. Nanocrystals of Cesium Lead Halide Perovskites (CsPbX$_3$, X = Cl, Br, and I): Novel Optoelectronic Materials Showing Bright Emission with Wide Color Gamut. *Nano Lett.* **2015**, *15*, 3692−3696.

(20) Jellicoe, T. C.; Richter, J. M.; Glass, H. F. J.; Tabachnyk, M.; Brady, R.; Dutton, S. E.; Rao, A.; Friend, R. H.; Credgington, D.; Greenham, N. C.; et al. Synthesis and Optical Properties of Lead-Free Cesium Tin Halide Perovskite Nanocrystals. *J. Am. Chem. Soc.* **2016**, *138*, 2941−2944.

(21) Zhang, F.; Zhong, H.; Chen, C.; Wu, X.; Hu, X.; Huang, H.; Han, J.; Zou, B.; Dong, Y. Brightly Luminescent and Color- Tunable Collidal CH$_3$NH$_3$PbX$_3$ (X = Br, I, Cl) Quantum Dots: Potential Alternatives for Display Technology. *ACS Nano* **2015**, *9*, 4533−4542.

(22) Guo, Y.; Liu, C.; Tanaka, H.; Nakamura, E. Air-Stable and Solution-Processable Perovskite Photodetectors for Solar-Blind UV and Visible Light. *J. Phys. Chem. Lett.* **2015**, *6*, 535−539.

(23) Yakunin, S.; Sytnyk, M.; Kriegner, D.; Shrestha, S.; Richter, M.; Matt, G. J.; Azimi, H.; Brabec, C. J.; Stangl, J.; Kovalenko, M. V.; et al. Detection of X-Ray Photons by Solution-Processed Lead Halide Perovskites. *Nat. Photonics* **2015**, *9*, 444−449.

(24) Wang, Y.; Li, X.; Song, J.; Xiao, L.; Zeng, H.; Sun, H. All-Inorganic Colloidal Perovskite Quantum Dots: A New Class of Lasing Materials with Favorable Characteristics. *Adv. Mater.* **2015**, *27*, 7101−7108.

(25) Sutherland, B.; Hoogland, S.; Adachi, M.; Wong, C. T. O.; Sargent, E. H. Conformal Organohalide Perovskites Enable Lasing on Spherical Resonators. *ACS Nano* **2014**, *8*, 10947−10952.

(26) Zhang, Q.; Ha, S. T.; Liu, X.; Sum, T. C.; Xiong, Q. Room-Temperature near-Infrared High-Q Perovskite Whispering-Gallery Planar Nanolasers. *Nano Lett.* **2014**, *14*, 5995−6001.

(27) Deschler, F.; Price, M.; Pathak, S.; Klintberg, L. E.; Jarausch, D.-D.; Higler, R.; Huttner, S.; Leijtens, T.; Stranks, S. D.; Snaith, H. J.; et al. High Photoluminescence Efficiency and Optically Pumped Lasing in Solution-Processed Mixed Halide Perovskite Semiconductors. *J. Phys. Chem. Lett.* **2014**, *5*, 1421−1426.

(28) Zhu, H.; Fu, Y.; Meng, F.; Wu, X.; Gong, Z.; Ding, Q.; Gustafsson, M. V.; Trinh, M. T.; Jin, S.; Zhu, X.-Y. Lead Halide Perovskite Nanowire Lasers with Low Lasing Thresholds and High Quality Factors. *Nat. Mater.* **2015**, *14*, 636−642.

(29) Shen, H.; Cao, W.; Shewmon, N. T.; Yang, C.; Li, L. S.; Xue, J. High-Efficiency, Low Turn-on Voltage Blue-Violet Quantum-Dot-Based Light-Emitting Diodes. *Nano Lett.* **2015**, *15*, 1211−1216.

(30) Hao, F.; Stoumpos, C. C.; Cao, D. H.; Chang, R. P. H.; Kanatzidis, M. G. Lead-Free Solid-State Organic−inorganic Halide Perovskite Solar Cells. *Nat. Photonics* **2014**, *8*, 489−494.

(31) Jang, D. M.; Park, K.; Kim, D. H.; Park, J.; Shojaei, F.; Kang, H. S.; Ahn, J.-P.; Lee, J. W.; Song, J. K. Reversible Halide Exchange Reaction of Organometal Trihalide Perovskite Colloidal Nanocrystals for Full-Range Band Gap Tuning. *Nano Lett.* **2015**, *15*, 5191−5199.

(32) Pellet, N.; Teuscher, J.; Maier, J.; Grätzel, M. Transforming Hybrid Organic Inorganic Perovskites by Rapid Halide Exchange. *Chem. Mater.* **2015**, *27*, 2181−2188.

(33) Akkerman, Q. A.; D'Innocenzo, V.; Accornero, S.; Scarpellini, A.; Petrozza, A.; Prato, M.; Manna, L. Tuning the Optical Properties of Cesium Lead Halide Perovskite Nanocrystals by Anion Exchange Reactions. *J. Am. Chem. Soc.* **2015**, *137*, 10276−10281.

(34) Nedelcu, G.; Protesescu, L.; Yakunin, S.; Bodnarchuk, M. I.; Grotevent, M. J.; Kovalenko, M. V. Fast Anion-Exchange in Highly Luminescent Nanocrystals of Cesium Lead Halide Perovskites (CsPbX$_3$, X = Cl, Br, I). *Nano Lett.* **2015**, *15*, 5635−5640.

(35) Mizusaki, J.; Arai, K.; Fueki, K. Ionic Conduction of the Perovskite-Type Halides. *Solid State Ionics* **1983**, *11*, 203−211.

(36) Tress, W.; Marinova, N.; Moehl, T.; Zakeeruddin, S. M.; Nazeeruddin, M. K.; Grätzel, M. Understanding the Rate-Dependent J−V Hysteresis, Slow Time Component, and Aging in CH$_3$NH$_3$PbI$_3$ Perovskite Solar Cells: The Role of a Compensated Electric Field. *Energy Environ. Sci.* **2015**, *8*, 995−1004.

(37) Yakunin, S.; Protesescu, L.; Krieg, F.; Bodnarchuk, M. I.; Nedelcu, G.; Humer, M.; De Luca, G.; Fiebig, M.; Heiss, W.; Kovalenko, M. V. Low-Threshold Amplified Spontaneous Emission and Lasing from Colloidal Nanocrystals of Caesium Lead Halide Perovskites. *Nat. Commun.* **2015**, *6*, 8056.

(38) Raino, G.; Nedelcu, G.; Protesescu, L.; Bodnarchuk, M. I.; Kovalenko, M. V.; Mahrt, R. F.; Stöferle, T. Single Cesium Lead Halide Perovskite Nanocrystals at Low Temperature: Fast Single-Photon Emission, Reduced Blinking and Exciton Fine Structure. *ACS Nano* **2016**, *10*, 2485−2490.

(39) Lignos, I.; Stavrakis, S.; Nedelcu, G.; Protesescu, L.; DeMello, A. J.; Kovalenko, M. V. Synthesis of Cesium Lead Halide Perovskite Nanocrystals in a Droplet-Based Microfluidic Platform: Fast Parametric Space Mapping. *Nano Lett.* **2016**, *16*, 1869−1877.

(40) Li, G.; Rivarola, F. W. R.; Davis, N. J. L. K.; Bai, S.; Jellicoe, T. C.; de la Peña, F.; Hou, S.; Ducati, C.; Gao, F.; Friend, R. H.; et al. Highly Efficient Perovskite Nanocrystal Light-Emitting Diodes Enabled by a Universal Crosslinking Method. *Adv. Mater.* **2016**, *28*, 3528−3534.

(41) Palazon, F.; Akkerman, Q. A.; Prato, M.; Manna, L. X-Ray Lithography on Perovskite Nanocrystals Films: From Patterning with Anion-Exchange Reactions to Enhanced Stability in Air and Water. *ACS Nano* **2016**, *10*, 1224−1230.

(42) Huang, H.; Chen, B.; Wang, Z.; Hung, T. F.; Susha, A. S.; Zhong, H.; Rogach, A. L.; et al. Water Resistant CsPbX$_3$ Nanocrysals Coated by Polyhedral Oligomeric Silsesquioxane and Their Use as Solid State Luminophores in All-Perovskite White Light-Emitting Devices. *Chem. Sci.* **2016**, *7*, 5699−5703.

(43) de Weerd, C.; Gomez, L.; Zhang, H.; Buma, W. J.; Nedelcu, G.; Kovalenko, M. V.; Gregorkiewicz, T. Energy Transfer Between Inorganic Perovskite Nanocrystals. *J. Phys. Chem. C* **2016**, *120*, 13310−13315.

(44) Dastidar, S.; Egger, D. A.; Tan, L. Z.; Cromer, S. B.; Dillon, A.; Liu, S.; Kronik, L.; Rappe, A. M.; Fafarman, A. T. High Chloride Doping Levels Stabilize the Perovskite Phase of Cesium Lead Iodide. *Nano Lett.* **2016**, *16*, 3563−3570.

(45) Egerton, R. Formulae for Light-Element Micro Analysis by Electron Energy-Loss Spectrometry. *Ultramicroscopy* **1978**, *3*, 243−251.

(46) de Mello, J.; Wittmann, H.; Friend, R. An Improved Experimental Determination of External Photoluminescence Quantum Efficiency. *Adv. Mater.* **1997**, *9*, 230−232.

(47) Kieslich, G.; Sun, S.; Cheetham, A. K. An Extended Tolerance Factor Approach for Organic−inorganic Perovskites. *Chem. Sci.* **2015**, *6*, 3430−3433.

(48) Förster, T. Transfer Mechanisms of Electronic Excitation. *Discuss. Faraday Soc.* **1959**, *27*, 7−17.

(49) Yang, S.; Liu, D.; Jiang, Y.; Teng, F.; Xu, Z.; Hou, Y.; Xu, X. Impact of Electric Fields on the Emission from Organic Light-Emitting Diodes Based on Polyvinylcarbazole (PVK). *J. Lumin.* **2007**, *122−123*, 614−616.

(50) Aleshin, A. N.; Sokolovskaya, A. D.; Shcherbakov, I. P.; Brunkov, P. N.; Ulin, V. P. Organic Light-Emitting Diodes Based on Polyvinylcarbazole Films Doped with Polymer Nanoparticles. *Phys. Solid State* **2013**, *55*, 675−680.